PAPER • OPEN ACCESS

Magnetic potential based formulation for linear and non-linear 3D RF sheath simulation

OPEN ACCESS
IOP Publishing | International Atomic Energy Agency
Nuclear Fusion
Nucl. Fusion **63** (2023) 026024 (12pp)
https://doi.org/10.1088/1741-4326/aca6f9

Magnetic potential based formulation for linear and non-linear 3D RF sheath simulation

S. Shiraiwa[1,*], N. Bertelli[1], W. Tierens[2], R. Bilato[2], J. Hillairet[3], J. Myra[4], H. Kohno[5], M. Poulos[1] and M. Ono[1]

[1] Princeton Plasma Physics Laboratory, Princeton, NJ 08540, United States of America
[2] Max-Planck-Institut für Plasmaphysik, Boltzmannstrasse 2, D-85748 Garching, Germany
[3] CEA, IRFM, F-13108 Saint-Paul-Lez-Durance, France
[4] Lodestar Research Corporation, 5055 Chaparral Ct., Suite 102, Boulder, CO 80301, United States of America
[5] Kyushu Institute of Technology, 680-4 Kawazu, Iizuka, Fukuoka 820-8502, Japan

E-mail: shiraiwa@princeton.edu

Received 8 August 2022, revised 28 October 2022
Accepted for publication 29 November 2022
Published 6 January 2023

Abstract

This paper reports a new numerical scheme to simulate the radio-frequency (RF) induced RF sheath, which is suitable for a large 3D simulation. In the RF sheath boundary model, the tangential component of the electric field (E_t) is given by the gradient of a scalar electric field potential. We introduce two additional scalar potentials for the tangential components of the magnetic field, which effectively impose the normal electric displacement (D_n) on the plasma sheath boundary condition via in-homogeneous Neumann boundary condition and constrain the tangential electric field on the surface as curl-free ($\nabla \times E_t = 0$). In our approach, the non-linear sheath impedance is formulated as a natural extension of the large thickness (or asymptotic) sheath limit ($D_n = 0$), allowing for handling both asymptotic and non-linear regimes seamlessly. The new scheme is implemented using the Petra-M finite element method analysis framework and is verified with simulations in the literature. The significance of non-linearity is discussed in various plasma conditions. An application of this scheme to asymptotic RF sheath simulation on the WEST ICRF antenna side limiters is also discussed.

Keywords: ICRF, full-wave simulation, RF sheath

(Some figures may appear in colour only in the online journal)

1. Introduction

Waves in the ion cyclotron range of frequency (ICRF) are widely used for heating fusion plasmas, and will continue to play a crucial role in heating of burning plasmas such as ITER [1, 2]. Many fusion ICRF heating experiments, however, reported detrimental accumulation of core impurity contents during ICRF operation [3–12]. On the surface of plasma-facing components, a thin electron-depleted layer called a sheath is formed. When the radio-frequency (RF) wave is injected into plasma, the non-linearity of the sheath I-V characteristic curve leads to the rectification of the RF electric field oscillation, creating a DC potential in the direction of accelerating ions to the material surface. With sufficiently high RF power injection, it is anticipated that the induced potential is much larger than what is determined by static sheaths resulting from thermal electrons. The consequent larger ion

* Author to whom any correspondence should be addressed.

bombardment has been considered a root cause of impurity increase during ICRF operation (RF sheath) [13, 14].

Our eventual goal is to build a computational model which can predict the RF sheath voltage and the associated impurity release in a fully integrated manner, where the ICRF wave propagation and absorption in hot core plasmas and geometrically complicated 3D antennas and plasma-facing components are all incorporated. Recent progress in RF full-wave simulation using massively parallel high-performance computers has already made it possible to simulate the ICRF wave propagation in tokamak plasmas using a 360-degree 3D volumetric computational domain with a realistic antenna model [15–17]. Therefore, it is a natural next step to consider integrating the RF rectified potential model. However, an appropriate form for including the RF sheath voltage development physics in such large-scale full-wave simulations is not yet fully developed.

Because the RF sheath is physically very thin, a boundary condition (BC) model to represent the sheath effects using zero thickness surface was proposed ('RF sheath BC') [18]. Using such an RF sheath BC in global RF field full-wave simulation has attracted considerable attention in the RF theory and computational community [19–28].

However, even with this simplification, using an RF sheath model in a 3D full-wave simulation is known to be difficult, as mentioned by several authors in the literature [13, 25, 28, 29]. Indeed, at present, a majority of published works are limited in 2D slab geometry simulation. And, in order to generate a sheath voltage prediction on a 3D surface, a technique of stacking multiple separate 2D sheath simulations has been commonly used, where each 2D slice is interfaced with 3D RF simulation without sheath BC [30, 31]. Another modelling technique was to introduce a finite thickness thin layer which is physically meshed to simulate the properties of an equivalent RF sheath [32]. In this approach, the sheath is a part of a simulation domain, not a boundary. It is yet to be demonstrated if this approach scales to large and geometrically complicated ICRF antennas on fusion devices.

There have been mainly two different approaches to using the RF sheath BC in global RF wave simulations [13]. One is to use the full form of parameterized non-linear sheath impedance [26, 33] ('full form' approach), and the other one is based on the expansion of wave field assuming a large sheath thickness ('expansion' approach) [20]. While those two approaches both aim to describe the same non-linear RF sheath physics, the mathematical representation appears rather different. As a result, they look somewhat disconnected. Therefore, we revisit those existing approaches and discuss the difference and commonality of these two models. The purpose of this step is neither to review the literature nor to find new physics behind the RF sheath rectification. Instead, our hope is to establish a better, organized perspective of existing RF sheath theory and to guide our development of a new RF sheath BC formulation useful in 3D full-wave simulations. We also discuss so-called DB BC ($D_\mathrm{n} = 0$ and $B_\mathrm{n} = 0$, where D_n and B_n are the normal component of the electric displacement and the magnetic field, respectively) [34–36]. It is mainly studied outside the fusion community, but actually has a close connection with the 'expansion' approach.

A main contribution of the present work is to propose a third way of formulating the RF sheath BC. It reformulates the RF sheath physics using the magnetic scalar potential and the Helmholtz decomposition. Mathematically, this formulation should yield an identical result to the simulation using the full form of the non-linear sheath impedance. However, in our view, it is more suited as a BC used in the boundary value problem of Maxwell equations. We implemented our approach with the open source Petra-M framework, which uses the MFEM library for the finite element method (FEM) discretization engine [37]. MFEM is an open-source finite element library which allows for using arbitrarily high-order discrete functional spaces in the de-Rham complex [38, 39]. Then, we verify it by benchmarking the simulation results with previous literature.

One can also view the proposed formulation as a generalization of the 'expansion' approach to a non-linear electromagnetic simulation. In fact, the new formulation can handle both non-linear and asymptotic limits seamlessly. We discuss the impact of non-linearity in various plasma parameters using the simulation geometries discussed in the existing literature. As mentioned earlier, our goal is to use the new formulation in a large 3D full-wave simulation with a realistic representation of plasma-facing components and RF antennas in tokamaks and stellarators. As a step towards this goal, we demonstrate the use of the asymptotic RF sheath model on the WEST 3D ICRF antenna side limiters [11, 12].

This paper is structured as follows. In the next section, we compare the existing two approaches of using the RF sheath BC in the global full-wave simulations. In the third section, we present our new formulation to implement the RF sheath BC in detail. The fourth section shows the simulation results including the model verification efforts and the initial application to realistic 3D simulations on the WEST tokamak. We summarize this paper, after a short discussion in section 5.

2. RF sheath models

A central idea of an RF sheath BC is that there is a scale separation between the size of space where the RF wave propagation is considered, and the thickness of the sheath layer on the material surface. This scale separation permits the sheath physics to be collapsed into a BC and justifies using an electrostatic approximation inside the sheath layer. This allows for defining the tangential component of RF electric field E_t on the plasma-sheath boundary as a gradient of sheath potential ϕ_e as

$$E_\mathrm{t} = -\nabla\phi_\mathrm{e}, \tag{1}$$

where ϕ_e is a scalar field defined on surface. Throughout this paper, except for equations (4)–(6), ∇, $\nabla\cdot$, $\nabla\times$ and Δ are differential operators on surface. The sheath potential ϕ_e is determined by the sheath impedance z_sh and the electric

displacement normal to the surface D_n ($\equiv \mathbf{D}\cdot\mathbf{n}$, where $\mathbf{n}$ is the normal vector on the plasma-sheath boundary) as follows [13],

$$\phi_e = i\omega D_n z_{sh}(|\phi_e|). \tag{2}$$

Here, z_{sh} is a function of local plasma parameters, such as density and temperature, and $|\phi_e|$. The latter is explicitly written to emphasize that the sheath impedance is a non-linear function of $|\phi_e|$. Note that we use ϕ_e for the RF driven sheath voltage, instead of V_{RF} found in the literature, in order to reserve the subscript for distinguishing several scalar potentials introduced in this paper.

In addition to the local RF wave amplitude, the sheath physics depends on local background plasma parameters. Thus, a series of sheath impedance models are developed, where the parametric dependence on background plasma properties are handled using a set of analytical functions [26, 33]. The latest version [33], called the generalized sheath impedance, includes electron, ion, and displacement current components, and includes the angle of the magnetic field with respect to the material surface, making it applicable to a broad range of situations found in fusion devices. In the RF sheath modelling using this 'full-form' approach, the boundary value problem of the Maxwell's equations is coupled with equation (1) under the constraints given by equation (2). In [22, 23, 26, 40], the rfSOL code was developed to solve such a coupled non-linear system in 2D slab geometry. The code uses the finite element discretization, and the resultant non-linear system is solved using the Newton–Raphson method.

The 'expansion' approach splits the fields into successive approximations, using the inverse of sheath thickness, δ. In [20], the expansion form was derived with the electrostatic approximation in the capacitive sheath limit ($\omega \gg \omega_{pi}$) in a stratified geometry. If we adopt the same approach, in an electromagnetic field, such an expansion would be written as follows,

$$\mathbf{E} = \mathbf{E}^{(0)} + (\lambda_{crit}/\delta)\mathbf{E}^{(1)} \ldots \tag{3}$$

where $\lambda_{crit}/\delta \ll 1$ is the non-dimensional expansion parameter, while λ_{crit} is a characteristic length discussed in [20]. The key point that as the sheath thickness increases, only the 0th order term, which is independent of the sheath thickness, remains important ('wide sheath' or 'asymptotic limit'). Formally, this asymptotic limit can be expressed as $z_{sh} \to \infty$, while maintaining ϕ_e finite. Then, from equation (2), it is seen that D_n has to be zero so that ϕ_e remains finite. As discussed below, the normal component of magnetic field, B_n ($\equiv \mathbf{B}\cdot\mathbf{n}$), is also zero, and this BC is summarized as $D_n = 0$ and $B_n = 0$. More recently, Tierens *et al.* [28] assessed this asymptotic case without using electrostatic approximation and formed exact solutions analytically and numerically.

Comparing 'full-form' and 'expansion' approaches, we notice that equation (1) is not used explicitly in the latter. Equation (2) is not necessary either if one uses the asymptotic limit. Instead, ϕ_e is evaluated afterwards by solving an auxiliary Poisson equation. In [20, 28], the right-hand side of the Poisson equation was given based on the divergence of the electric displacement. However, we can also evaluate this right-hand side by the surface divergence of E_t without the approximation discussed in section 5.3 in [13]. Then, the important difference is that while the 'full-form' approach uses the relationship in equation (1) to compute the E_t from ϕ_e, the 'expansion' approach uses it in the opposite direction.

In the literature, the 'expansion' approach only demonstrated a complete non-linear simulation with the electro-static approximation [20]. What we consider here is to take the electromagnetic field solution obtained in the asymptotic limit ($D_n = 0$ and $B_n = 0$) and use it in the non-linear iteration. Our motivation to seek such a path is the potential numerical robustness of integration, as opposed to the differentiation, by reducing a small spatial scale error. It is rather obvious that once ϕ_e is obtained from E_t, we could use equation (2) to evaluate D_n. At this point, D_n would not be zero, therefore we need to impose such non-zero D_n for solving the Maxwell equation making the complete loop of non-linear iteration.

It is illustrative to compare the difference between non-linear iteration schemes used in the 'full-form' approach and what we are considering here using figure 1. In the RF sheath simulation, the global electric field simulation (E(3D) in the figure) and the sheath potential ϕ_e are coupled via $\mathbf{E}_t$ and D_n (four boxes in the figure). The goal of non-linear iterations is to find a set of these four parameters which satisfies the physics relationship (equations (1) and (2)) self-consistently. The left one is the 'full form' approach. Four parameters are linked in the way following the loop in the clockwise direction. Namely, D_n is an output from the RF solver, which is used to compute ϕ_e. Then, E_t is evaluated using the gradient of ϕ_e, which is then fed to the RF field solver as the Dirichlet BC. This approach is reasonable if the electric field is expressed using a continuous element and thus the normal component of displacement behaves well. However, when using a basis function which defines a discontinuous D_n, the gradient is not well-defined.

Our approach goes over the loop in the opposite direction as shown on the right of the figure. The input to the RF solver is D_n (Neumann BC). Consequently, E_t is an output from the RF solver. Note that, in the RF solver, the electric field is further constrained to satisfy $\nabla \times \mathbf{E}_t = 0$, so that it guarantees that ϕ_e exists. Then, D_n is computed using equation (2).

In order to use our new non-linear iteration scheme, however, we need to impose D_n in the RF field solver. Note that this is not a common form for imposing the BC. As discussed below, a natural way for imposing the BC is to define it by using the tangential components of an electric field or magnetic field. It is worth mentioning, however, that the asymptotic limit ($D_n = 0$ and $B_n = 0$) is identical to the DB boundary in [34–36]. It is important to realize that although this asymptotic limit is sometimes referred as 'insulating limit', it is different form the insulating BC ($\mathbf{H}_t = 0$), which would have been implemented without complexity. Indeed, [28] showed that there are two independent solutions, one of which does not satisfy the insulating BC. As far as we are aware, however,

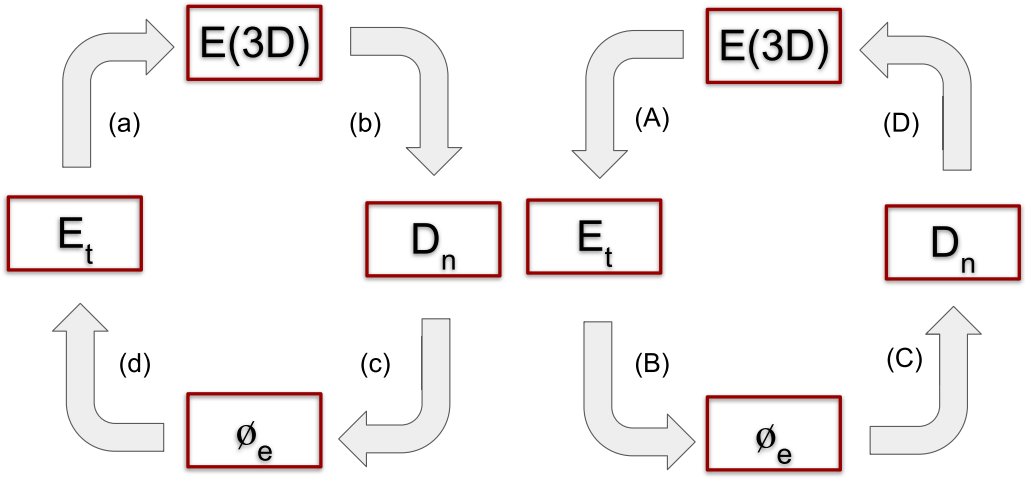

Figure 1. Comparison between two iteration schemes. E(3D) is a step to solve the Maxwell equation (equation (4)). The rest are the evaluation on the RF sheath BC. [Left] (*a*) $\mathbf{E}_t$ is imposed as Dirichlet BC, (*b*) $\mathbf{D}_n$ is evaluated from RF field, (*c*) sheath potential is evaluated and (*d*) $\mathbf{E}_t$ is given by the gradient of ϕ_e. [Right] (*A*) $\mathbf{E}_t$ is read from RF field, (*B*) ϕ_e is computed from $\mathbf{E}_t$, (*C*) $\mathbf{D}_n$ is evaluated from ϕ_e, and (*D*) D_n is imposed to compute RF electric field.

it hasn't been discussed how this DB BC is implemented in a regular 3D FEM RF solver setting using the H(curl) elements [41, 42] (see also Ch. 8 of [43]) .

Therefore, in the next section, we first derive the formulation based on a magnetic scalar potential to impose the asymptotic limit. Then, we extend the asymptotic sheath BC to the case with non-zero D_n by introducing the second scalar potential. Two scalar potentials used here define curl-free and divergence-free components of tangential magnetic field, and thus it is an application of the Helmholtz decomposition. Such a decomposition is always possible when the boundary shape is simply connected. Indeed, the decomposition already appears in the form of the analytical expression derived in [28] (see equation (46) and the following paragraph).

3. Formulation using magnetic potential

3.1. Radio frequency wave physics model in Petra-M

The radio frequency module in Petra-M is designed as a general purpose electromagnetic field solver. It allows for the solution of the Maxwell's equations for the electric field in the frequency domain using a broad range of BCs via a user friendly graphical interface [44]. This implementation is based on the well-know, widely used weakform formulation of the boundary value problem of the Maxwell equation [43, 45]. Therefore, we briefly summarize its physics level description as an introduction to our magnetic potential based RF sheath formulation.

In Petra-M, we use the convention of $\exp(-i\omega t)$ for time dependence. The Maxwell equation is written as follows,

$$\nabla\times\left(\frac{1}{\boldsymbol{\mu}}\nabla\times\mathbf{E}\right)-(\omega^2\,\boldsymbol{\epsilon}+i\omega\boldsymbol{\sigma})\mathbf{E}=i\omega\mathbf{J}_{\rm ext}, \tag{4}$$

where $\mathbf{J}_{\rm ext}$ is an externally imposed current, ω is the angular frequency, $\boldsymbol{\varepsilon}$, $\boldsymbol{\mu}$, and $\boldsymbol{\sigma}$ are the permittivity, permeability and conductivity, respectively. In order to specify the physics problem uniquely in a bounded domain Ω, On the boundary of Ω, $\partial\Omega$, one of following two BCs are imposed.

$$\mathbf{n}\times\mathbf{E}=\mathbf{E}_0 \;\; on \;\; \partial\Omega_1 \tag{5}$$

$$\mathbf{n}\times\left(\frac{1}{\boldsymbol{\mu}}\nabla\times\mathbf{E}\right)+\gamma\mathbf{n}\times\mathbf{n}\times\mathbf{E}=\mathbf{Q} \;\; on \;\; \partial\Omega_2 \tag{6}$$

where $\partial\Omega=\partial\Omega_1\cap\partial\Omega_2$, $\mathbf{E}_0$ and $\mathbf{Q}$ are known vector field, and γ is a known scalar parameter. Equation (5) specifies the tangential component of electric field (Dirichlet BC), while equation (6) is called the Robin BC.

In equation (4), $\boldsymbol{\epsilon}$ represents the plasma response to the RF field. In the present work, we use the cold plasma approximation for $\boldsymbol{\varepsilon}$. On the local coordinate system, in which the background magnetic field is oriented in the Z direction, $\boldsymbol{\varepsilon}$ is given by [46]

$$\boldsymbol{\epsilon}=\begin{pmatrix}\mathcal{S} & -i\mathcal{D} & 0\\ i\mathcal{D} & \mathcal{S} & 0\\ 0 & 0 & \mathcal{P}\end{pmatrix} \tag{7}$$

where, using the angular frequency ω, the cyclotron frequency ω_{cs} and plasma frequency ω_{ps} for particle species s, the Stix notations are given as

$$\mathcal{S}\equiv 1-\sum_{\rm s}\frac{\omega_{\rm ps}^2}{\omega^2-\omega_{cs}^2} \tag{8}$$

$$\mathcal{D}\equiv\sum_{\rm s}\frac{\omega_{\rm ps}^2\omega_{cs}}{\omega(\omega^2-\omega_{\rm cs}^2)} \tag{9}$$

$$\mathcal{P} \equiv 1 - \sum_{\mathrm{s}} \frac{\omega_{\mathrm{ps}}^2}{\omega^2}. \tag{10}$$

In Petra-M, the electric field is discretised using the H(curl) basis functions and the Galerkin method is used to construct a linear system from these equations. Spatial dependence of the background plasma parameters appears in ω_{ps} and ω_{cs}, which is incorporated by the quadrature integration during linear system construction. Notice that physics quantities appearing in equations (5) and (6) are tangential components of **E** and **H**. Therefore, we need to translate the sheath BC to a formulation conformal to these forms.

3.2. Asymptotic sheath BC

We consider the situation that a portion of the computational domain boundary ($\partial\Omega_3$) is given by the asymptotic sheath BC figure 2. We further restrict our consideration to the case $\partial\Omega_3$ is a simply connected boundary surface and is surrounded by a perfect electric conductor (PEC, i.e. $\mathbf{E}_{\mathrm{t}} = 0$ on the circumference of $\partial\Omega_3$). Then, we can express this BC in the following three pairs of conditions, which are equivalent to each other. The first form is based on the normal component of fields, given by

$$D_{\mathrm{n}} = 0, \tag{11}$$

$$B_{\mathrm{n}} = 0. \tag{12}$$

The second form is, using the Ampére and Faraday's laws,

$$\nabla \times \mathbf{H}_{\mathrm{t}} = 0 \tag{13}$$

$$\nabla \times \mathbf{E}_{\mathrm{t}} = 0, \tag{14}$$

where subscript t indicates the field components tangential to the boundary $\partial\Omega_3$. Note that ∇ here is an operator acting on the plasma-sheath surface. The third form uses scalar potentials, given by

$$\mathbf{H}_{\mathrm{t}} = -\nabla\phi_{\mathrm{h}} \tag{15}$$

$$\mathbf{E}_{\mathrm{t}} = -\nabla\phi_{\mathrm{e}}. \tag{16}$$

Because these three are equivalent, we have the freedom to mix them conveniently. $\mathbf{H}_{\mathrm{t}}$ directly relates to $\frac{1}{\boldsymbol{\mu}}\nabla \times \mathbf{E}$ appearing in equation (6), and thus, equation (15) can be implemented using $\gamma = 0$ and $\mathbf{Q} = 0$ in equation (6). Also, the tangential component of the electric field is well defined in the H(curl) element space. Therefore, we choose the following pair.

$$\mathbf{H}_{\mathrm{t}} = -\nabla\phi_{\mathrm{h}} \tag{17}$$

$$\nabla \times \mathbf{E}_{\mathrm{t}} = 0. \tag{18}$$

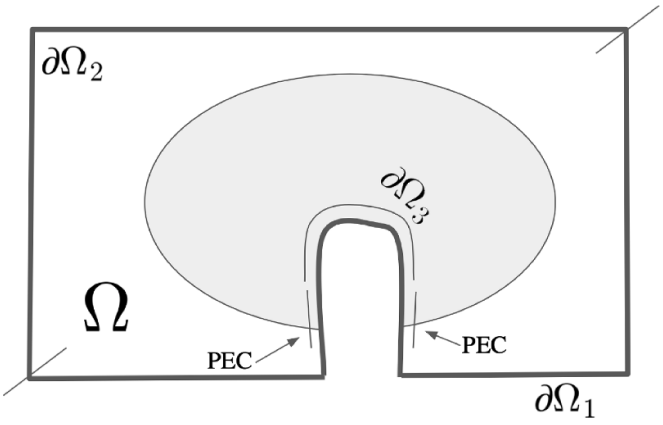

Figure 2. Schematics of simulation geometry. Simulation domain Ω. is surrounded by boundary, $\partial\Omega$, which is defined either by equation (5) (on $\partial\Omega_1$) or equation (6) (on $\partial\Omega_2$). A part of boundary facing plasma ($\partial\Omega_3$) is defined by the sheath BC discussed in this paper. Note that a part of $\partial\Omega_1$ connecting to $\partial\Omega_3$ is assumed to be PEC ($\mathbf{E}_0 = 0$ in equation (5)).

Note that ϕ_{h} on the right-hand side is unknown. In other words, we redefine our physics problem as a problem to find the vector electric field **E** and the additional scalar function ϕ_{h} simultaneously. This is possible because $\nabla \times \mathbf{E}_{\mathrm{t}} = 0$ is an additional scalar equation and the number of unknowns and number of equations matches. One could reach the same pair starting from constraining the Maxwell equations to satisfy equation (18) using a Lagrange multiplier. The discussion here gives the physical meaning of the multiplier.

Taking the divergence of equation (16) yields

$$\Delta\phi_{\mathrm{e}} = -\nabla \cdot \mathbf{E}_{\mathrm{t}}. \tag{19}$$

Thus, once electric field is computed, we can obtain the electric scalar potential, which satisfies equation (16), by solving this Poisson equation with an appropriate BC. Because our sheath BC is surrounded by PEC, ϕ_{e} is constant on the boundary. In the asymptotic limit, we have a freedom to choose this constant arbitrarily. In the non-linear case discussed next, however, this constant would be determined by the non-linear iteration.

One may wonder that, when using the H(curl) finite element, this right-hand side is not well defined, since $\mathbf{E}_{\mathrm{t}}$ in the H(curl) space is discontinuous in the direction normal to the surface mesh boundary. Proper treatment is to eliminate this divergence by using integration by parts after multiplying by a test function. One will see that two boundary integration terms from equation (19) cancel out, leaving the contribution from the domain integration.

3.3. Nonlinear sheath BC

In this case, we have the non-linear relation between D_{n} and ϕ_{e} (equation (2)). Because we have already evaluated ϕ_{e} via equation (19), we use this relationship to evaluate D_{n} as follows,

$$D_{\mathrm{n}} = -i\phi_{\mathrm{e}}/\omega z_{\mathrm{sh}}(|\phi_{\mathrm{e}}|). \tag{20}$$

The non-linear sheath BC has $D_n \neq 0$ on $\partial\Omega_3$, and the relationship equation (17) does not hold. The last step of our derivation is to use D_n as a BC for the RF solver. We split $\mathbf{H}_t$ into two terms (the Helmholtz decomposition) as follows,

$$\mathbf{H}_t = -\nabla\phi_h + \mathbf{n}\times\nabla\varphi_h, \tag{21}$$

where the first term is the irrotational (curl-free) component, which is the same as the asymptotic limit (equation (17)), and the new second term is the solenoidal (divergence-free) component. Taking the curl of this equation yields

$$\nabla\times\mathbf{H}_t = -\nabla^2\,\varphi_h = i\omega D_n \tag{22}$$

where the second relationship is used to obtain φ_h from D_n. As before, ϕ_h is solved together with E in the same way as the asymptotic case. Therefore the change from the asymptotic limit is to add the new divergence-free contribution to the Neumann BC (equation (6)), when solving for the Maxwell's equations.

One can see that this new approach incorporates naturally the asymptotic limit. It is given as the first non-linear iteration when $\phi_e = 0$ is used as an initial value. It makes the direct comparison between the asymptotic limit and the non-linear sheath rather straightforward, without requiring to implement the DB boundary separately.

3.4. Numerical smoothing of sheath potential

As far as the RF sheath physics is concerned, the set of equations discussed in previous sections should be sufficient. Indeed, in the majority of simulation cases presented in the following section, the non-linear iteration converged even by using a simple fixed-point iteration. However, under certain conditions, we observed a significant slow down of the convergence without using the following numerical smoothing. A similar smoothing of the tangential electric field is discussed in [22, 23]. In our implementation, we apply a diffusion smoothing on the sheath potential, and use the smoothed potential as an argument of the sheath impedance.

$$D_n = \frac{\phi_e}{i\omega z_{sh}(\langle\phi_e\rangle)} \tag{23}$$

$$\langle\phi_e\rangle - a_s^2\,\nabla^2\,\langle\phi_e\rangle = \phi_e \tag{24}$$

where a_s is the smoothing width. In the simulations presented in this paper, $a_s = 5$ mm is used when it is necessary. We also performed a sensitivity test (not shown here), confirming that the result does not change more than a few percent. A further discussion on this smoothing is given in section 5.

4. Numerical results

4.1. Verification of implementation

The formulation we discussed in the previous section was implemented in the Petra-M finite element analysis framework. In our implementation, a linear system to go around the loop shown in figure 1(left) is constructed as a block matrix. This resultant non-linear equation is solved by either a fixpoint iteration or a damped Newton–Raphson method, using the MUMPS direct [47, 48] solver as a linear solver. In order to verify the implementation, our results are compared with simulation models discussed in the literature.

In the asymptotic regime, we use a vacuum simulation discussed in [28] to which an analytical solution was obtained. The FEM mesh geometry is the unstructured tetrahedral mesh with a uniform mesh size of 7 mm as shown in figure 3(left). The asymptotic sheath BC is imposed on the Y-Z surface indicated in the figure. The computed $\mathbf{E}_y$, $\mathbf{E}_z$, and ϕ_e are shown in figure 4, which agree well with figures 8, 9, and 10 in [28].

Since both D_n and B_n are only weakly constrained in our linear system, it is important to check the convergence of these two. Figure 5 shows how $|E_n|$ and $|B_n|$ change together with the sheath potential solution for three different finite element basis function polynomial orders, $P = 2$, 4, and 6. Since this case is vacuum, we show E_n instead of D_n. It is clearly seen that while ϕ_e results are the same among three cases, $|E_n|$ and $|B_n|$ continue to decrease to zero, as anticipated. The convergence of $|E_n|$ and $|B_n|$ up to $P = 6$ is also shown on the right, showing a nearly order of magnitude reduction of $|E_n|$ and $|B_n|$ with each element order refinement.

In the non-linear regime, we performed an extensive comparison with the series of 2D slab simulations using the rfSOL code discussed in [26, 27], where the generalized non-linear sheath impedance composed of electron, ion and displacement current contributions is used [33]. Note that the complete dataset for the series of simulations in these references is publicly available (see URL links in references), making them well suited for the RF sheath code benchmarks.

An example of parallel electric field ($E_{||}$) profiles computed by Petra-M using our new formulation is shown in figure 6. This example was prepared as a benchmark against figure 11 in [27]. The simulation geometry and plasma parameters are exactly the same as the reference (detailed in the figure captions). However, in the Petra-M simulation, the shaped sheath BC edge was meshed by 72 grid points and then the inside of the computational domaichann was meshed using the unstructured triangles. We also used the H(curl) elements and a higher order basis function between $P = 3$ to 6, while the reference cases are performed using a quadrilateral mesh with the second order continuous elements. The result shows excellent agreement with the reference simulation including the wave amplitude, phase, and wavelength.

Figure 14 in [27] shows the sheath potential when the sheath is generated on a flat and shaped (with bump) surface using the geometries shown in figure 3(right). Figure 7 shows the sheath potential computed by Petra-M (lines), benchmarking again the rfSOL simulations (circles). Again, simulation geometry and all plasma parameters are identical to the ones used in [27], except for the mesh and FEM element basis function and order. This comparison shows an excellent agreement within $\sim$1% difference of $\max(|\phi_e|)$.

We note, however, that two high K_{max} cases with the shaped wall geometry ($K_{max} = 800$ and 1000 A m^{-1} in figure 7(right)) are slow to converge even using a damped Newton method.

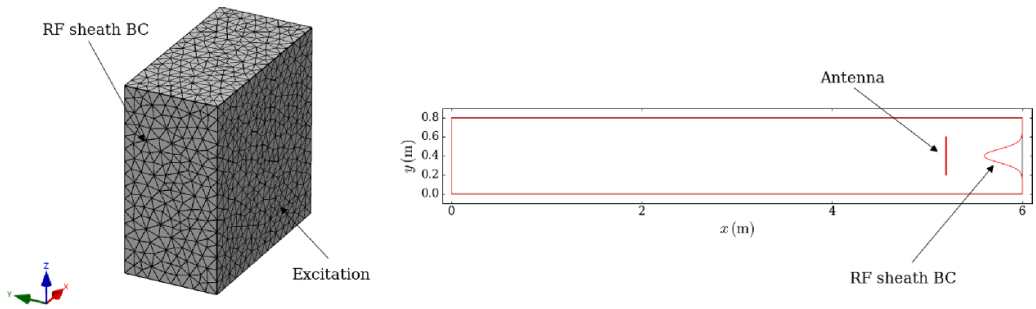

Figure 3. Finite element geometry used in comparison with [28] (left) and [27] (right). The sheath BC is imposed on the boundaries indicated by arrows. On the left one, the wave is excited on the X-Z surface using the essential BC. On the right, the wave is excited by the RF currents imposed on the antenna.

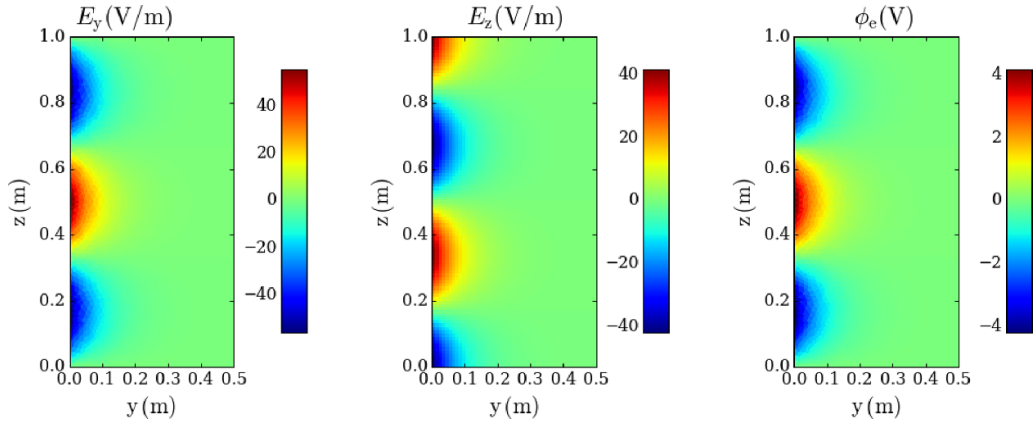

Figure 4. Sheath potential ϕ_e, and z-component and y component of electric field ($\mathbf{E}_z$, and $\mathbf{E}_y$) for the asymptotic sheath model.

Moreover, the obtained electric field profile for such cases shows a numerical pollution by very short wavelength oscillations. So far, the good agreement shown in the figure was obtained only with the numerical smoothing discussed in section 3.4, where the smoothing distance is chosen to be much smaller than the bump height ($a_s = 5$ mm).

In [22, 23], a similar grid-scale oscillation and numerical smoothing on the surface electric field is also discussed. While the rfSOL code did not need to use the smoothing for those particular cases in figure 7, a spatial smoothing of sheath potential could be justified based on the same physics insight mentioned in [22, 23]. In fact, at a high antenna current, due to a shallow intersection angle of the magnetic field to the sheath BC, the projection of electron jitter distance ($qE_{||}/m_e\omega^2$) tends to be large (∼a few mm). Additionally, spatial smoothing could naturally occur, when the RF simulation is coupled with the DC potential field simulation [20].

4.2. Comparison of asymptotic and non-linear RF sheath BC

Our new formulation facilitates using both asymptotic limit and non-linear sheath BCs. Therefore, we compare the sheath potentials predicted by two models using a range of plasma parameters in figure 8.

These simulations prepared using the same geometry and parameters discussed in figures 7 and 11 of [26]. The flat sheath BC geometry in 2D, similar to the one shown with black in figure 3(right), is used, and the antenna currents are swept in a wide range to see the effect of non-linearity (see figure caption and [26] for the details of plasma parameters). The asymptotic prediction is linearly proportional to the antenna current amplitude, as anticipated. The non-linear simulation predicts a more complicated dependence. Generally speaking, the non-linearity tends to reduce the sheath potential at low antenna current compared to the asymptotic model. Then, at a sufficiently high antenna current, the sheath potential tends to recover the linearity. This behaviour is reasonable, considering that the asymptotic limit is a wide sheath width limit.

The difference between the non-linear and the asymptotic prediction is, however, plasma parameter dependent and it could be large even at a very high ϕ_e. One key parameter seems to be the proximity to the slow wave resonance ($S = 0$) which, in the case of ICRF is closely connected with the presence of the sheath-plasma resonance (see section 6.2 of [13] and references therein). Sheath-plasma resonance conditions, if present, lie at intermediate antenna current, and can result in very large sheath potentials. The simulations in figure 8 are performed at a density sufficiently separated from the slow wave resonance density ($\sim 3 \times 10^{17}\mathrm{m}^{-3}$). With the plasma parameters discussed in figure 7 in which the density is very close to the resonance density ($2.49 \times 10^{17}\,\mathrm{m}^{-3}$), we

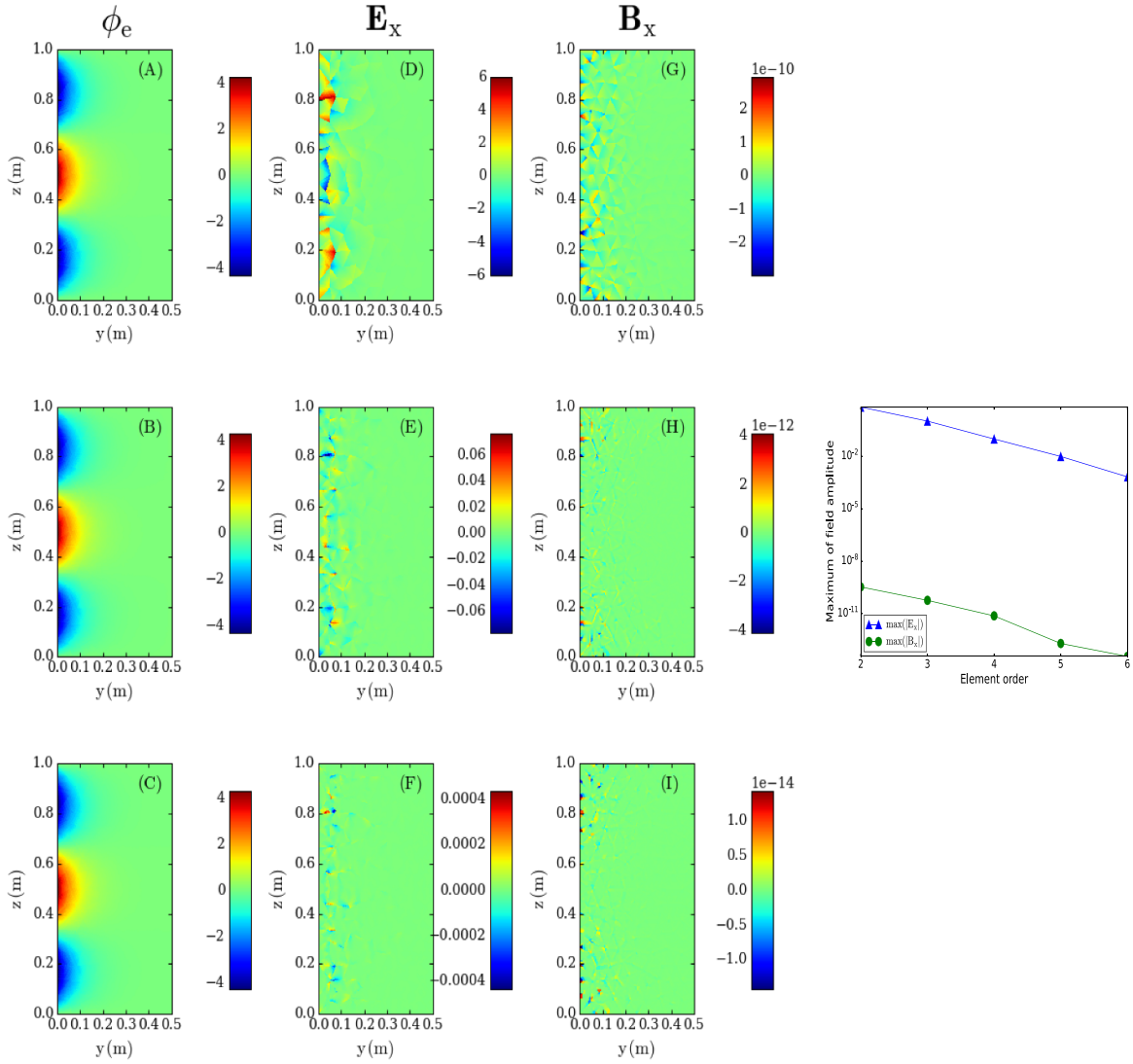

Figure 5. Convergence of ϕ_e (shown in A, B, and C panels), $\mathbf{E}_x$ (shown in D, E, and F panels), and $\mathbf{B}_x$ (shown in G, H, and I panels) on the RF sheath boundary. The polynomial orders of $P = 2$, 4 and 6 are used on the top, middle and bottom rows, respectively.

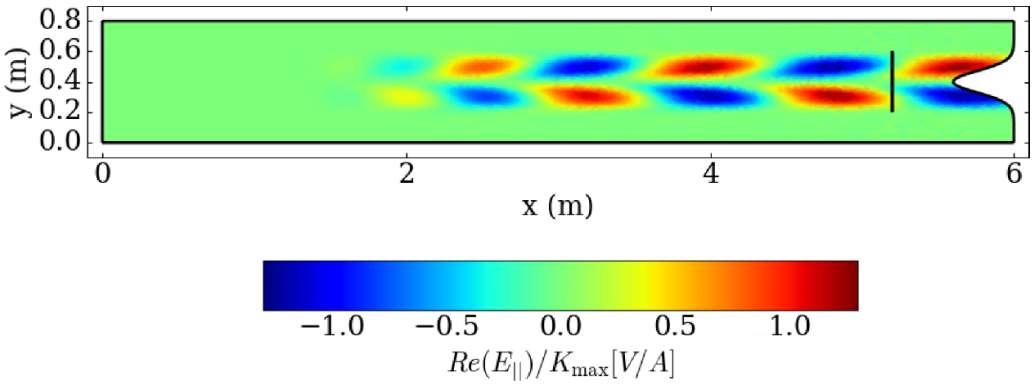

Figure 6. Parallel electric field $E_{||}$ computed by Petra-M for the same conditions used in figure 11 in [27]. A shaped RF sheath boundary was located on the right side of the antenna. The antenna location is indicated by the vertical line inside the computational domain. Plasma parameters are the same as the reference, namely: electron density of $n_e = 1 \times 10^{17} \mathrm{m}^{-3}$, background magnetic field of $\mathbf{B} = (4, 0, 0)$ T, and antenna current of $J_y(y) = K_{max} \cos^2(\frac{\pi}{L_{ant}}(y - y_0))$ with $K_{max} = 600\ \mathrm{A\,m}^{-1}$.

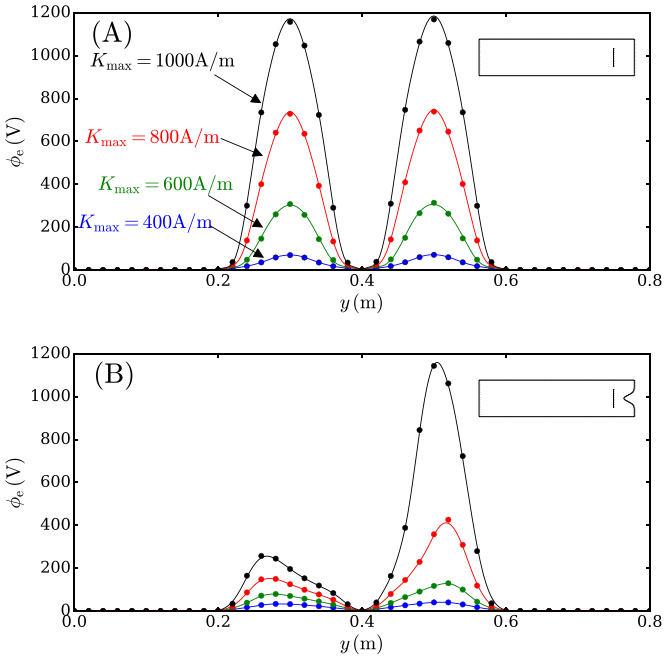

Figure 7. Comparison of ϕ_e computed by our formulation (solid lines) and the reference results in [27] (circles) using the flat (*A*) and shaped sheath boundary (*B*), respectively. See [27] for the details of plasma parameters used in these simulations.

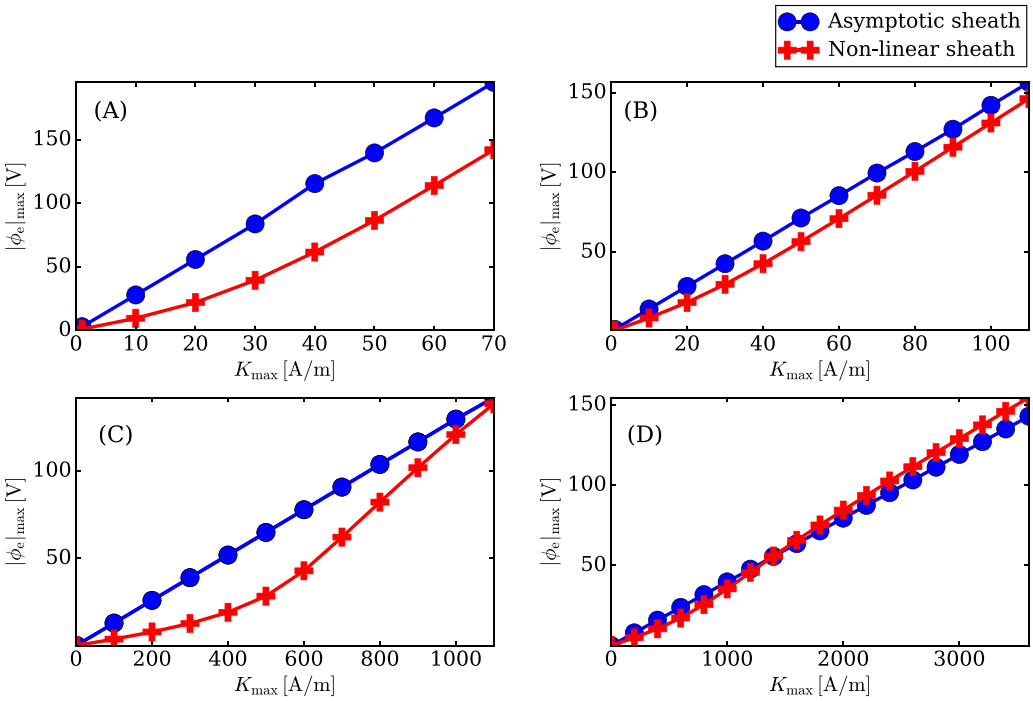

Figure 8. The sheath potential predicted by asymptotic (blue circle) and non-linear (red cross) sheath model. The geometry and plasma parameters discussed in figures 7 and 11 in [26] are used. The background magnetic field is $\mathbf{B} = (1, 0, 0)$ T, and (*A*) $k_z = 160$ m^{-1}, $n_e = 1.0 \times 10^{17}$ m^{-3}, (*B*) $k_z = 320$ m^{-1}, $n_e = 1.0 \times 10^{17}$ m^{-3}, (*C*) $k_z = 160$ m^{-1}, $n_e = 2.0 \times 10^{18}$ m^{-3}, and (*D*) $k_z = 320$ m^{-1}, $n_e = 2.0 \times 10^{18}$ m^{-3} are used, respectively.

found that the difference between asymptotic and non-linear prediction is significant even at $\phi_e \sim 1$ kV (not shown). This observation agrees qualitatively what is shown in equation (4.17) in [20], which shows the expansion parameter is inversely proportional to $\sqrt{S}$.

4.3. Initial application on the WEST ICRF side limiter

As a demonstration of computing the RF sheath potential with realistic tokamak antenna geometry, we applied the new RF sheath implementation to the side wall of the WEST ICRF

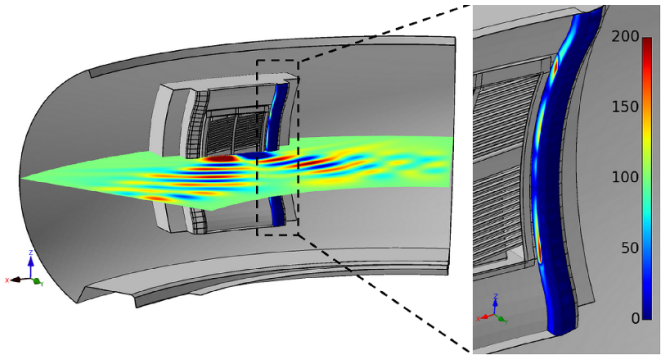

Figure 9. ICRF propagation and asymptotic sheath potential induced on the WEST side limiter. 1MW of ICRF power at 53 MHz injected. Uniform SOL density of 3×10^{17} m^{-3}, and parabolic core density profile with the peak density of 4×10^{19} m^{-3} is used.

antenna. We used a WEST ICRF antenna 3D model generated from the CAD geometry, in figure 9. For this demonstration, we used the asymptotic sheath model to avoid the need of solving a large linear system many times. The edge density is chosen to be 3×10^{17}m^{-3}, which is much larger than the resonance density ($\sim3\times n_{\rm res}$), while a parabolic density profile with the central density of 4×10^{19}m^{-3} is used inside the last closed flux surface. As for a magnetic field profile, an equilibrium profile with the central magnetic field 3.5 T is used. Note that we are using the cold plasma approximation equation (7) even in the core region and enhanced collisions are used to mimic a strong single pass power absorption.

On the enlarged view in figure 9 (left), the computed RF sheath potential for 1 MW of ICRF power injection is shown. It can be seen that there are two large peaks in the top and bottom regions of the side limiter. There is also a smaller peak slightly above the mid-plane. Interestingly, the predicted sheath potential is in the range of 100–200 V, suggesting that the RF sheath could be indeed a physics mechanism relevant to the ICRF-induced impurities. Although this initial demonstration was not meant to make a direct comparison with experiments, it is worth mentioning that the predicted sheath potential profile is in qualitative agreement with the IR camera and visible spectroscopy signal reported in [49] (figure 4(*a*)).

5. Discussion

As mentioned in the introduction, several previous works indicated the difficulty of using the RF sheath in global RF full-wave simulations. Our test implementation of the 'full-form' approach, which was attempted before implementing the proposed formulation, was not satisfactory either, due to the difficulty of achieving reliable non-linear convergence.

In our view, it appears that the difficulty arises from two aspects. First, the de-facto standard choice of basis function in the RF electric field solver is the H(curl) edge element, and accurately evaluating $D_{\rm n}$ is at least non-trivial if not impossible. This is because the H(curl) element does not hold the information of the normal component of fields on the degree of freedoms (DoFs) associated with the boundary. Second, such a normal component is discontinuous on the mesh boundary and therefore the gradient can not be well defined in the finite element sense. It is likely that evaluating $\phi_{\rm e}$, and especially $\mathbf{E}_{\rm t}$, from such $D_{\rm n}$ tends to introduce a numerical noise, causing a slow down of the non-linear convergence. Note that the 2D rfSOL code, which we used for verification, uses the continuous elements and does not have this difficulty.

Our alternative approach circumvents these difficulties. It uses $E_{\rm t}$ from the RF solver, this information can be simply gathered from the DoFs directly associated with the boundary. Instead of taking the gradient of $\phi_{\rm e}$, integrating $\mathbf{E}_{\rm t}$ (the Poisson equation) is also numerically advantageous, because the integration acts like a low pass filter, making it less sensitive to short-scale length errors.

It is worth to discuss the small wavelength oscillations in the two high current cases on figure 7(right), which we observed when the smoothing is not used. While we do not have a enough support to believe that they are a real wave branch, it may be too early to exclude such a possibility. One possibility is a surface wave mode. The RF sheath is an electron depleted thin layer, creating the sign change of dielectric property. Thus, it may allow for a surface wave mode which can propagate only along the boundary similar to that discussed in [19, 50]. The sheath plasma wave resonance is in fact just such a wave mode localized near the plasma-sheath boundary.

We emphasize, however, that these two high current cases are the only two extreme cases, for which we observed the difference in code convergence behaviour. Although we only focus on a limited number of cases in this paper, we performed benchmark simulations using all relevant simulations discussed in the above two references. In general, we obtained an excellent agreement with the difference of a few per cent, despite the fact that the two approaches are very different not only from the formulation point of view, but also from the FEM implementation including the type of basis function used to represent the fields. This gives good confidence in the physics formulation and implementation. A broader code benchmark effort of the RF sheath model including other simulation codes is in progress in the RF SciDAC project [51] and will be published in the future.

Our eventual goal is to predict the non-linear sheath potential induced on plasma-facing components of fusion devices using a realistic 3D antenna geometry and PFC models in a torus. The result demonstrated with WEST ICRF antenna geometry in this paper is, however, performed using the asymptotic limit. Extending the present 3D asymptotic simulation to the non-linear regime is straightforward from the mathematical formulation point of view. However, it requires solving a large linear system a number of times, and therefore we consider it outside the scope of the present work. Furthermore, an important ingredient of such an integrated RF sheath simulation is to use a more accurate plasma wave power absorption model in the tokamak core region. One possibility is our previous work to integrate the TORIC spectral solver in the core with the FEM-based edge simulation [52]. However, it needs to be expanded to handle non-linearity in the edge region,

and this point will be addressed in our future work. Additionally, we are planning to work closely with the WEST team to perform a detailed comparison between the code prediction and experiments. A crucial measurement for such validation includes the RF rectified potential in SOL regions.

6. Summary

In this paper, a new formulation based on magnetic field scalar potentials is developed in order to incorporate the RF sheath BC in 3D FEM-based RF full-wave simulations. In the new formulation, we evaluate the sheath potential by integrating the tangential electric field, instead of evaluating the tangential electric field from the gradient of the sheath potential. From the sheath potential, we compute the normal component of displacement, which is then used to constrain the global RF field simulation using a form of non-homogeneous Neumann BC. The relationship between the existing two approaches for the RF sheath BC, 'full-form' and 'expansion' approaches, is also discussed. A clear perceptive of existing theories guided us for developing our third way, and from this perspective, our approach can be viewed as an extension of the 'expansion' approach, eliminating the electrostatic wave field approximation.

The new approach was implemented in the Petra-M FEM analysis platform, and benchmarked against several cases in the literature [26–28]. Overall, excellent agreement was observed. Additionally, our approach facilitates both the asymptotic ('wide' sheath) and non-linear sheath models in a seamless manner, allowing for direct comparison of the two models more easily.

Using the newly developed formulation, the RF sheath potential on the WEST side wall limiter was predicted in the asymptotic limit. As far as the authors are aware, this is the first demonstration of using the RF sheath BC directly in a 3D electromagnetic field simulation without relying on simplification techniques such as stacking the 2D simulations. The predicted sheath potential profile ranges from 100 to 200 V for 1 MW of injected ICRF power, and it has two large peaks near the top and bottom parts of the limiter surface and a smaller peak near the mid-plane.

The present work paves a path to include the RF-induced sheath voltage prediction in a large-scale integrated RF full-wave simulation.

Acknowledgment

Authors (S.S. and N.B.) appreciate Drs L. Colas and G. Urbanczyk for a detailed discussion on the WEST ICRF experiments. Discussions with the RF-SciDAC team (Center for Simulation of Wave–Plasma Interactions) are gratefully acknowledged. This work was supported by the U.S. Department of Energy under Contract No. DE-AC02-09CH1146. The United States Government retains a non-exclusive, paid-up, irrevocable, world-wide license to publish or reproduce the published form of this manuscript, or allow others to do so, for United States Government purposes. This research also used resources of the National Energy Research Scientific Computing Center (NERSC), a U.S. Department of Energy Office of Science User Facility located at Lawrence Berkeley National Laboratory, operated under Contract No. DE-AC02-05CH11231.

ORCID iDs

S. Shiraiwa https://orcid.org/0000-0001-5249-0441
N. Bertelli https://orcid.org/0000-0002-9326-7585
J. Hillairet https://orcid.org/0000-0002-1073-6383
J. Myra https://orcid.org/0000-0001-5939-8429
M. Ono https://orcid.org/0000-0001-9849-9417

References

[1] Schneider M., Artaud J.-F., Bonoli P., Kazakov Y., Lamalle P., Lerche E., Van Eester D. and Wright J. 2017 *EPJ Web Conf.* **157** 03046
[2] ITER Research Plan 2018 The ITER Research Plan (ITR 18-003)
[3] Wukitch S., Lipschultz B., Marmar E., Lin Y., Parisot A., Reinke M., Rice J. and Terry J. 2007 *J. Nucl. Mater.* **363–365** 491
[4] Wukitch S.J., LaBombard B., Lin Y., Lipschultz B., Marmar E., Reinke M.L. and Whyte D.G. 2009 *J. Nucl. Mater.* **390-391** 951
[5] Perkins R.J. *et al* 2012 *Phys. Rev. Lett.* **109** 045001
[6] Bobkov V. *et al* 2013 *Nucl. Fusion* **53** 093018
[7] Bobkov V. *et al* 2016 *Nucl. Fusion* **56** 084001
[8] Czarnecka A. *et al* 2012 *Plasma Phys. Control. Fusion* **54** 074013
[9] Lerche E. *et al* 2005 *J. Nucl. Mater.* **463** 634
[10] Perkins R.J., Hosea J.C., Taylor G., Bertelli N., Kramer G.J., Luo Z.P., Qin C.M., Wang L., Xu J.C. and Zhang X.J. 2019 *Plasma Phys. Control. Fusion* **61** 045011
[11] Hillairet J. *et al* 2021 *Nucl. Fusion* **61** 096030
[12] Bucalossi J. *et al* 2022 *Nucl. Fusion* **62** 042007
[13] Myra J.R. 2021 *J. Plasma Phys.* **87** 905870504
[14] Colas L. *et al* 2022 *Nucl. Fusion* **62** 016014
[15] Shiraiwa S. *et al* 2020 *28th IAEA-FEC Conf.* (available at: https://conferences.iaea.org/event/214/)
[16] Bertelli N. *et al* 2020 *AIP Conf. Proc.* **2254** 030001
[17] Bertelli N., Shiraiwa S. and Ono M. 2022 *Nucl. Fusion* **62** 126046
[18] D'Ippolito D.A. and Myra J.R. 2006 *Phys. Plasmas* **13** 102508
[19] Myra J.R. and D'Ippolito D.A. 2009 *Plasma Phys. Control. Fusion* **52** 015003
[20] Colas L., Jacquot J., Heuraux S., Faudot E., Crombé K., Kyrytsya V., Hillairet J. and Goniche M. 2012 *Phys. Plasmas* **19** 092505
[21] Jacquot J. *et al* 2014 *Phys. Plasmas* **1** 061509
[22] Kohno H., Myra J.R. and D'Ippolito D.A. 2015 *Phys. Plasmas* **22** 072504
[23] Kohno H., Myra J.R. and D'Ippolito D.A. 2016 *Phys. Plasmas* **23** 089901 (erratum)
[24] Myra J.R. and D'Ippolito D.A. 2015 *Phys. Plasmas* **22** 062507
[25] Colas L., Lu L.-F., Křivská A., Jacquot J., Hillairet J., Helou W., Goniche M., Heuraux S. and Faudot E. 2017 *Plasma Phys. Control. Fusion* **59** 025014
[26] Kohno H. and Myra J.R. 2017 *Comp. Phys. Comm.* **220** 129–142
[27] Kohno H. and Myra J.R. 2019 *Phys. Plasmas* **26** 022507
[28] Tierens W., Urbanczyk G., Colas L. and Usoltceva M. 2019 *Phys. Plasmas* **26** 083501

[29] Jacquot J. 2013 Self-consistent non-linear description of radio-frequency wave propagation and of the edge of a magnetized plasma *PhD Thesis* Université de Lorraine, (France)
[30] Křivská A. *et al* 2019 *Nucl. Mater. Energy* **19** 324
[31] Tierens W., Jacquot J., Bobkov V., Noterdaeme J.M. and Colas L. 2017 *Nucl. Fusion* **57** 116034
[32] Beers C.J. *et al* 2021 *Phys. Plasmas* **28** 093503
[33] Myra J.R. 2017 *Phys. Plasmas* **24** 072507
[34] Kress R. and Leis R. 1986 *Math. Methods Appl. Sci.* **8** 0170–4214
[35] Lindell I.V. and Sihvola A. 2019 *Boundary Conditions in Electromagnetics* (New York: Wiley-IEEE Press)
[36] Kress R. 2021 *SIAM J. Math. Anal.* **53** 3661–80
[37] Shiraiwa S., Wright J.C., Bonoli P.T., Kolev T. and Stowell M. 2017 *EPJ Web Conf.* **157** 03048
[38] Anderson R. *et al* 2021 *Comput. Math. Appl.* **81** 42
[39] MFEM (available at: http://mfem.org)
[40] Kohno H., Myra J.R. and D'Ippolito D. 2012 *Comput. Phys. Commun.* **183** 2116
[41] Whitney H. 1957 *Geometric Integration Theory* (Princeton, NJ: Princeton University Press)
[42] Nedelec J.C. 1980 *Numer. Math.* **35** 315
[43] Jin J. 2014 *Element Method in Electromagnetics* 3rd edn (New York: Wiley)
[44] Shiraiwa S., Fredian T., Hillairet J. and Stillerman J. 2016 *Fusion Eng. Des.* **112** 835
[45] Bondeson A., Rylander T. and Ingelström P. 2000 *Computational Electromagnetics* (Berlin: Springer)
[46] Stix T.H. 1992 *Waves in Plasmas* (New York: Springer)
[47] Amestoy P., Duff I. and L'Excellent J.Y. 2000 *Comput. Methods Appl. Mech. Eng.* **184** 501–20
[48] Amestoy P.R., Duff I.S., L'Excellent J.Y. and Koster J. 2001 *SIAM J. Matrix Anal. Appl.* **23** 15–41
[49] Urbanczyk G., Fedorczak N., Gunn J., Colas L., Li J.G. and Wang K. 2021 *Nuclear Mater. Energy* **26** 100925
[50] Tierens W. and Colas L. 2021 *J. Plasma Phys.* **87** 905870405
[51] Wright J.C. *et al* 2021 Development of a non-linear rf sheath benchmark suite *Pittsburgh, PA (8–12 November 2021) 63rd Annual Meeting of the APS Division of Plasma Physics* (available at: https://meetings.aps.org/Meeting/DPP21/Session/GP11.10)
[52] Shiraiwa S., Wright J.C., Lee J.P. and Bonoli P.T. 2017 *Nucl. Fusion* **57** 086048